Food Chemistry: X 23 (2024) 101689

Contents lists available at ScienceDirect

Food Chemistry: X

journal homepage: www.sciencedirect.com/journal/food-chemistry-x

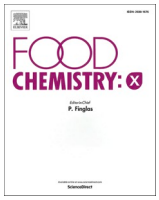

Characterization and stability of lycopene-loaded high internal phase emulsion stabilized by ovalbumin-chitosan complexes

Dan Wang [a], Junmiao Zhang [b], Lei Zhong [b], Cheng Yang [a], Xuejian Zhang [a], Qiuhui Hu [b], Lianfu Zhang [a,*]

[a] State Key Laboratory of Food Science and Resources, Jiangnan University, Wuxi, Jiangsu 214122, China
[b] College of Food Science and Technology, Nanjing Agricultural University, Nanjing 210095, China

ARTICLE INFO

Keywords:
Ovalbumin
Chitosan
High internal phase emulsion
Lycopene
Storage stability

ABSTRACT

Lycopene, a carotenoid with numerous physiological benefits, particularly in its *Z*-isomer form, faces challenges in its application due to low chemical stability. To address this limitation, high internal phase emulsion was successfully synthesized using ovalbumin-chitosan complexes. The aim was to enhance the stability of lycopene including *Z*-lycopene. The solubility, particle size, ζ-potential and uniformity of the mixture were dependent on pH value and biopolymer proportion. Notably, optimal ovalbumin-chitosan complex formation occurred at pH 2.5 with a ratio of 4:1 resulting in the highest solubility and optimal uniformity which contributed to its superior emulsification properties. Evaluation of encapsulating efficiency and loading amount revealed 98.19% and 1.7661 mg/g respectively for lycopene in ovalbumin-chitosan stabilized emulsions, inhibiting the transformation from *Z*-lycopene to (all-*E*)-lycopene. The encapsulated lycopene possessed UV stability where retention rate remained high at 81.86%. The retention rate was up to 65.37% and 41.82% at 45 °C and 80 °C, respectively.

1. Introduction

Lycopene, a liposoluble carotenoid with powerful antioxidation, plays a vital role in protecting the eyes from oxidative damage and preventing degenerative diseases (Falsafi et al., 2022; Saini et al., 2020). The excellent physiological activity of lycopene is mainly derived from a highly unsaturated hydrocarbon structure. Eleven conjugated double bonds and two non-conjugated double bonds create an electron-rich environment responsible for absorbing long waves and quenching singlet oxygen, thereby giving lycopene excellent oxidation resistance. The unique structure of lycopene allows it to have not only (all-*E*)-lycopene in nature but also dozens of *Z*-lycopene, of which (5*Z*)-, (9*Z*)-, (13*Z*)- and (15*Z*)-lycopene are the most commonly found in foods (Saini et al., 2019). In human serum and tissues, over 50.0% of lycopene is *Z*-lycopene, which is better absorbed than (all-*E*)-lycopene due to the shorter length of the *Z*-lycopene and its high solubility in mixed micelles. Compared with (all-*E*)-lycopene, *Z*-lycopene has higher antioxidant activity, and showed more outstanding inhibition on the prevention of benign prostatic hyperplasia in mice (Zou et al., 2014). However, two main challenges limit the practical application of lycopene. One of the two is that the highly unsaturated hydrocarbon structure of lycopene makes it prone to chemical reactions. The degradation of lycopene when exposed to high temperature, oxygen, and light can lead to its fading and loss of biological activity, greatly affecting its application in different food related systems. Another is that over 90% of lycopene from natural fruits and vegetables exists in an (all-*E*)-lycopene. Heating treatment is the main method for the *Z*-lycopene, but the transformed *Z*-lycopene is not stable (Zahari et al., 2023). Therefore, it is necessary to develop appropriate encapsulation system, especially using food-grade materials, to ensure that *Z*-lycopene has good physical and chemical stability in different environments such as production, storage, transportation, and final product utilization (Sampaio et al., 2019).

Various encapsulation systems, including solid lipid nanoparticles, nanostructured lipid carriers, and emulsions, have been developed for encapsulating lycopene (Banasaz et al., 2020; Mwangi et al., 2020). Solid lipid nanoparticles embed lycopene into this type of solid oil for storage, exhibiting high encapsulation efficiency. However, the disadvantage is that the loading amount is small, and lipids are prone to losing stability during the storage process of encapsulating active substances due to crystal transformation (Nazemiyeh et al., 2016). The nanostructured lipid carrier loaded with lycopene exhibits excellent stability during storage and has the advantages of solid lipid nanoparticles, due

* Corresponding author.
E-mail address: lianfu@jiangnan.edu.cn (L. Zhang).

https://doi.org/10.1016/j.fochx.2024.101689
Received 7 April 2024; Received in revised form 18 July 2024; Accepted 21 July 2024
Available online 22 July 2024

to its particle structure prepared by mixing solid lipids with liquid lipids (Sharma et al., 2021). However, both types of nanoparticles have the disadvantage of poor controlled-release performance. Emulsions can not only make the release of bioactive compounds in the gastrointestinal tract more controllable (Rostamabadi et al., 2019), but also improve their dispersion in food and reduce the negative impact on food sensory properties. Thus, it has become one of the most convenient and effective vehicles for encapsulating and delivering lycopene, especially in liquid formulations such as beverages. Nanoemulsions and Pickering emulsions effectively protect lycopene from external factors, showcasing improved stability (Gao et al., 2023; Zhao et al., 2020). Compared to nanoemulsions, pickering emulsions with gel-like structures ensure a better storage stability, due to its capacity of higher oil phases. Higher oil fractions were beneficial for controlling lycopene release during gastrointestinal digestion. However, emulsions are thermody-namically unstable, have short time span of usability and leads to creaming and breaking of emulsion because of improper formulation.

To overcome these limitations, high internal phase emulsions (HIPEs) have emerged as promising encapsulation systems (Rehman et al., 2024). HIPEs, characterized by a high internal phase volume ratio (≥74%), offer advantages over traditional emulsions in efficiently encapsulating and isolating lipophilic bioactive substances like lycopene (Chen, Sun, et al., 2023). Ovalbumin (OVA) has been utilized as a stabilizer for HIPEs due to its ability to prevent unfolding and aggregation (Thareja et al., 2020). However, OVA's hydrophilicity poses challenges in certain environmental conditions, prompting the exploration of combining it with polysaccharides like chitosan (CS) to enhance stability (Gao et al., 2021; Sharkawy et al., 2020).

The incorporation of CS into HIPEs, forming OVA-CS complexes, represents an innovative approach to improve stability and rheological properties (Zhang et al., 2023). This strategy offers multiple functionalities, including effective thickening and reinforcement of the network structure. In order to improve the stability of emulsions loading carotenoid, the formula including protein, emulsifier and polymer has been used (Wei et al., 2021), but the effect did not meet expectations. First, the emulsion prepared by non-ionic emulsifier has too large particle size, which will affect the stability of emulsion, which would affect the stability of carotenoid in the emulsions (Wang et al., 2020). Then, non-ionic emulsifier and polymer belong to food additives in China, so excessive dosage poses safety issues. The use of natural macromolecular complexes in food is green and safe. Compared to other emulsions encapsulating *Z*-lycopene (Murakami et al., 2022; Sun et al., 2022), the HIPEs show higher encapsulation efficiency up to 98.19%, and HIPEs prepared under acidic conditions has good acid resistance. Despite the influence of light and temperature, the *Z*-lycopene is unlikely to transform into (all-*E*) lycopene due to the unique gel network structure of HIPEs, while the *Z*-lycopene decreased by 50% in other emulsions. Meanwhile, the particle size (17.32 μm) of HIPEs is smaller than that (>20 μm) of the emulsions prepared by the same type of macromolecule (Xia et al., 2024), indicating that HIPEs have great potential in digestion and absorption.

In this study, we explore the effects of the OVA to CS ratio and pH value on the interaction between OVA and CS, as well as the emulsifying properties of resulting OVA-CS complexes. Additionally, we characterize the morphological and interfacial properties of the complexes to deepen our understanding of their structure and behavior. Subsequently, we systematically examine the influence of OVA-CS complexes on the formation, microstructure, and stability of HIPEs, considering varying mass concentrations and lycopene concentrations. This comprehensive analysis aims to contribute valuable insights to the field of HIPE-based encapsulation systems for lipophilic bioactive substances.

2. Materials and methods

2.1. Materials

(All-*E*)-lycopene (>98% purity) was supplied by North China Pharmaceutical Co., Ltd. (Shijiazhuang, China). Corn oil was bought from Yihai Kerry Co., Ltd. (Shanghai, China). OVA, CS and fluorescent dyes (Nile Red and FITC) were obtained from Sigma-Aldrich, Inc. (Shanghai, China). Calcofluor white (CW) were purchased from Kulaibo Technology Co., Ltd. (Beijing, China). All the other chemicals were of analytical grade.

2.2. Preparation of OVA-CS complexes

The chitosan (CS) was added to a 1.0% acetic acid solution and stirred for 12 h to obtain an aqueous chitosan solution. Subsequently, ovalbumin (OVA) was dissolved in deionized water and stirred for 4 h to prepare an OVA solution. The pH value of OVA solution was 6.16. The CS solution was then mixed with the OVA solution under magnetic stirring, resulting in a series of OVA-CS solutions with varying ratios (the concentration of CS or OVA was fixed at 1.0%). And the ratios of OVA to CS were set as 9:1, 6:1, 4:1, 2:1, and 1:1. The initial pH values corresponding to this series of OVA-CS solutions were 4.54, 4.57, 4.52, 4.37, and 4.18. To adjust the pH values of the OVA-CS solutions from pH 2 to pH 7, HCl (1 M) and NaOH (1 M) solutions were used. An IKA magnetic stirrer operating at a speed of 500 rpm was employed to prepare the series of OVA-CS solutions.

2.3. Effect of pH on the formation of OVA-CS complexes

2.3.1. Interaction of OVA and CS

The turbidity determination of OVA-CS solution was conducted following the method described by Xiong et al. (Xiong et al., 2017). The pH of the OVA-CS solution was adjusted to 7 using a 0.5 mol/L NaOH solution, and to 2 using a 1.5 mol/L HCl solution. For every change in solution pH within the range of 0.05–0.2, a volume of 200 μL was pipetted out. Subsequently, the mixed solutions at different pH values were transferred into separate wells of a 96-well plate and subjected to repeated measurements until reaching approximately pH 2. The absorbance of each mixed solution was measured at a wavelength of 600 nm with distilled water as the blank control. To ensure accurate measurement of dynamic pH changes during titration, magnetic stirring at a speed of 200 rpm was employed throughout the entire process.

2.3.2. Particle size and ζ-potential

The average particle size and ζ-potential of OVA-CS solutions were determined using a Zetasizer Nano ZS90 (Malvern, America) at 25 °C. When the average particle size was determined, the OVA-CS solutions were diluted with deionized water at a ratio of 1:500 (*v*/v) to mitigate potential interference from multiple particles, and the pH value was readjusted to maintain the pH constant. The OVA-CS solutions were directly used for ζ-potential measurement to maintain the potential.

2.3.3. Microstructural analysis

Distribution of OVA and CS in solution was visualized and documented using a confocal laser scanning microscope (CLSM 710, Zeiss, Germany) at a magnification of 400×. Prior to imaging, OVA and CS were respectively stained with FITC (1 mg/mL in ethanol solution) and CW (1 mg/mL in ethanol solution), as described by Zhao et al. (Zhao et al., 2021). The samples were examined under laser excitation at wavelengths of 488 nm or 405 nm.

2.3.4. Emulsifying activity (EAI) and emulsifying stability (ESI)

The sample was prepared by homogenizing 15 mL of OVA-CS solutions and 5 mL of corn oil using an IKA Ultra-Turrax T18 homogenizer (Staufen, Germany) operating at 12000 rpm for 3 min (Yao et al., 2022).

Subsequently, at the time points of 0 min and 10 min, a volume of 100 μL from the bottom of the tube was extracted and added to a solution containing SDS (0.1%, *w/v*) with a final volume of 5 mL. The turbidity measurement was performed by determining the absorbance at a wavelength of 500 nm after appropriate dilution. The EAI and ESI were calculated using the following formulas:

$$\mathrm{EAI}\ \left(\mathrm{m^2/gprotein}\right) = \frac{2.303 \times 2 \times \mathrm{N} \times \mathrm{A_0}}{\mathrm{C} \times (1-\varphi) \times 10000 \times \theta} \quad (1)$$

N is the dilution factor. φ is the volume fraction of the oil phase. C is the protein concentration of the sample in the solution (g/mL). θ is the light path of colorimetric cell. A_0 is the absorbance value at the 0 min.

$$\mathrm{ESI}\ (\%) = \frac{\mathrm{A_0}}{\mathrm{A_0} - \mathrm{A_{10}}} \times 100 \quad (2)$$

A_0 is the absorbance value at 0 min. A_{10} is the absorbance value at 10 min.

2.3.5. The three-phase contact angle and dynamic interfacial tension

The three-phase contact angle and interfacial tension of OVA-CS complexes were determined using a DSA 25 droplet shape analyzer (KRÜSS, Germany) following a modified version of the previously established method (Zhao et al., 2021). To measure the three-phase contact angle, freeze-dried OVA-CS complexes were compressed into 2 mm thick tablets and immersed in cold corn oil. Excess oil on the tablet surface was removed using filter paper before gently placing a 4 μL Milli-Q water drop onto the tablet surface. Droplet shape images were captured at a rate of 10 pictures per second using a camera and fitted to the Young-Laplace equation for profile analysis. For determination of interfacial tension, undiluted OVA-CS solutions (30 μL) were injected into cold corn oil to form drops. The adsorption process was then monitored over time to evaluate dynamic interfacial tension.

2.4. Preparation of lycopene-loaded HIPEs stabilized by OVA-CS complexes

The *Z*-lycopene was prepared according to Wang et al. (Wang et al., 2022). (All-*E*)-Lycopene was dissolved in acetone at a concentration of 0.1 mmol/L, while aluminum chloride with a concentration of 100 mmol/L was dissolved in deionized water. A 0.25 mL aluminum chloride solution was charged into a round bottom flask containing 10 mL lycopene solution for the water bath thermal reaction. The isomerization reaction was conducted at 40 °C for 120 min under darkness. After the reaction is completed, the aluminum ions are separated using a liquid separation method, adding n-hexane and an equal volume of distilled water to the separating funnel. Then, discard the aqueous phase and repeat adding distilled water for three times. A rotary evaporator and nitrogen blowing instrument were used to dry the solution. After drying, the *Z*-lycopene was stored at −20 °C for use.

The *Z*-lycopene, comprising 0.2%, 0.3%, and 0.4% concentrations by weight, was blended with corn oil, respectively. Subsequently, the oil suspensions underwent rapid heating in an oil bath maintained at a temperature of 174 °C (Chen et al., 2021). The OVA-CS solutions were prepared at concentrations of 3.0%, 4.0%, and 5.0% by weight. The HIPEs were prepared by homogenizing a mixture of lycopene corn oil (7.5 g) and OVA-CS solution (2.5 g) using an IKA Ultra-Turrax T18 homogenizer (Staufen, Germany) operating at 12000 rpm for 3 min (Xu et al., 2020). The HIPEs comprised of 0.2%, 0.3%, and 0.4% lycopene were achieved. And the lycopene-loaded HIPEs stabilized by 3.0%, 4.0%, and 5.0% OVA-CS complexes were also achieved. Similarly, the HIPEs stabilized by OVA were prepared as control.

2.5. Characterization of lycopene-loaded HIPEs stabilized by OVA-CS complexes

2.5.1. Particle size

The average particle size (d_{10}, d_{50}, d_{90}, $d_{4,3}$, and $d_{3,2}$) and distribution of HIPEs were determined using a laser particle size analyzer (Microtrac S3500, America) employing wet dispersion technology. Deionized water was utilized as the dispersant during the experimental procedure. The refractive indices of corn oil and the dispersant were 1.47 and 1.33 respectively.

2.5.2. Microstructure analysis

The microstructure of HIPEs was examined and documented using a confocal laser scanning microscope (LSM 710, Zeiss, Germany) at a magnification of 400×. Prior to observation, the oil phases in the emulsion were stained with Nile Red (1 mg/mL; dissolved in ethanol) as described by Zhao et al. (Zhao et al., 2021). Laser excitation light at a wavelength of 535 nm was employed for sample visualization.

2.5.3. Encapsulation efficiency and loading capacity

The aliquots (0.05 g) of HIPEs were collected and mixed with 5 mL of ethyl acetate. A 1000 μL pipette was used to repeatedly blow until lycopene in the sample was completely dissolved. The resulting solution was then filtered using a disposable syringe and an organic filter head with a pore size of 0.22 μm to eliminate any potential sediments. Subsequently, the filtrate was collected for lycopene quantification. To determine the content of lycopene, the HPLC conditions employed in our previous study were slightly modified for this work (Yang et al., 2021). Lycopene analysis was performed using an Alliance 2695 HPLC system (Waters Corp., Shanghai, China) equipped with a PDA detector (2998, Waters Corp.). Separation was achieved on a polymeric C30 column (YMC Carotenoids, 5 μm, 250 × 4.6 mm, Shanghai, China). A sample injection volume of 20 μL and a detection wavelength of 471 nm were utilized. The flow rate was maintained at 1 mL/min. The chromatography conditions were as follows: solvent A, methanol/H_2O (95:5, *v*/v); solvent B, MTBE/methanol (80:20, v/v). 0–20 min, 45% B; 20–28 min, to 50% B; 28–34 min, to 95% B; 34–40 min, to 100% B; 40–45 min, to 45% B.

Encapsulation efficiency and loading amount of lycopene in the HIPEs were evaluated using the following formulas:

$$\mathrm{EE}\ (\%) = \frac{\text{total quantity of LYC in corn oil}}{\text{total quantity of LYC in HIPE}} \times 100 \quad (3)$$

$$\mathrm{LA}\ (\mathrm{mg/g}) = \frac{\text{Encapsulated quantity of LYC}}{\text{total quantity of HIPE}} \quad (4)$$

2.6. Stability of lycopene-loaded HIPE stabilized by OVA-CS complexes

To avoid microbial contamination during storage, 0.5% ascorbic acid was used in OVA-CS solution, and the samples were stored in sterilized bottles with a capacity of 5 mL, then the bottles were filled with carbon dioxide. For the chemical stability assessment, the retention rates of lycopene in HIPEs during a 30-day storage period at 25 °C, 45 °C, 80 °C, and 25 °C with light were determined. The aliquots (0.05 g) of HIPEs were collected at specific intervals (every 10 d) and vigorously mixed with 5 mL of ethyl acetate. A 1000 μL pipette was used to repeatedly blow until lycopene in the sample was completely dissolved. The resulting solution was then filtered using a disposable syringe and an organic filter head with a pore size of 0.22 μm to eliminate any potential sediments. Subsequently, the filtrate was collected for lycopene quantification. Similarly, lycopene in corn oil was also obtained and quantified following the aforementioned method. The HPLC technique was employed to determine the lycopene content, utilizing a calibration curve for accurate quantification purposes. As a control, fully dissolved lycopene with an equivalent concentration as that in HIPEs was utilized.

The retention rate of lycopene was calculated using the following equation:

$$\text{Retention rate } (\%) = \frac{\text{lycopene content in the sample}}{\text{initial lycopene content}} \times 100 \quad (5)$$

2.7. Statistic analysis

The experiments were conducted in triplicate, and the results were expressed as means ± standard deviation (SD). Duncan's multiple-range test was employed to determine significant differences between mean values. Correlations were assessed using one-way ANOVA with the SPSS 13.0 statistical software (IBM Inc., Armonk, New York, USA). A probability value of $P < 0.05$ was considered statistically significant.

3. Results and discussion

3.1. The formation of OVA-CS complex

3.1.1. Turbidity

Soluble OVA-CS complexes were successfully formed at pH 2.5, evident from minimal turbidity (Fig. 1A). This phenomenon was attributed to electrostatic repulsion between the cationic amino groups on CS and positive charges on the OVA surface, aligning with findings by Hasanvand et al. (Hasanvand & Razavi, 2023). As the OVA:CS mass ratios shifted to 9:1, 6:1, and 4:1, turbidity sharply increased with rising

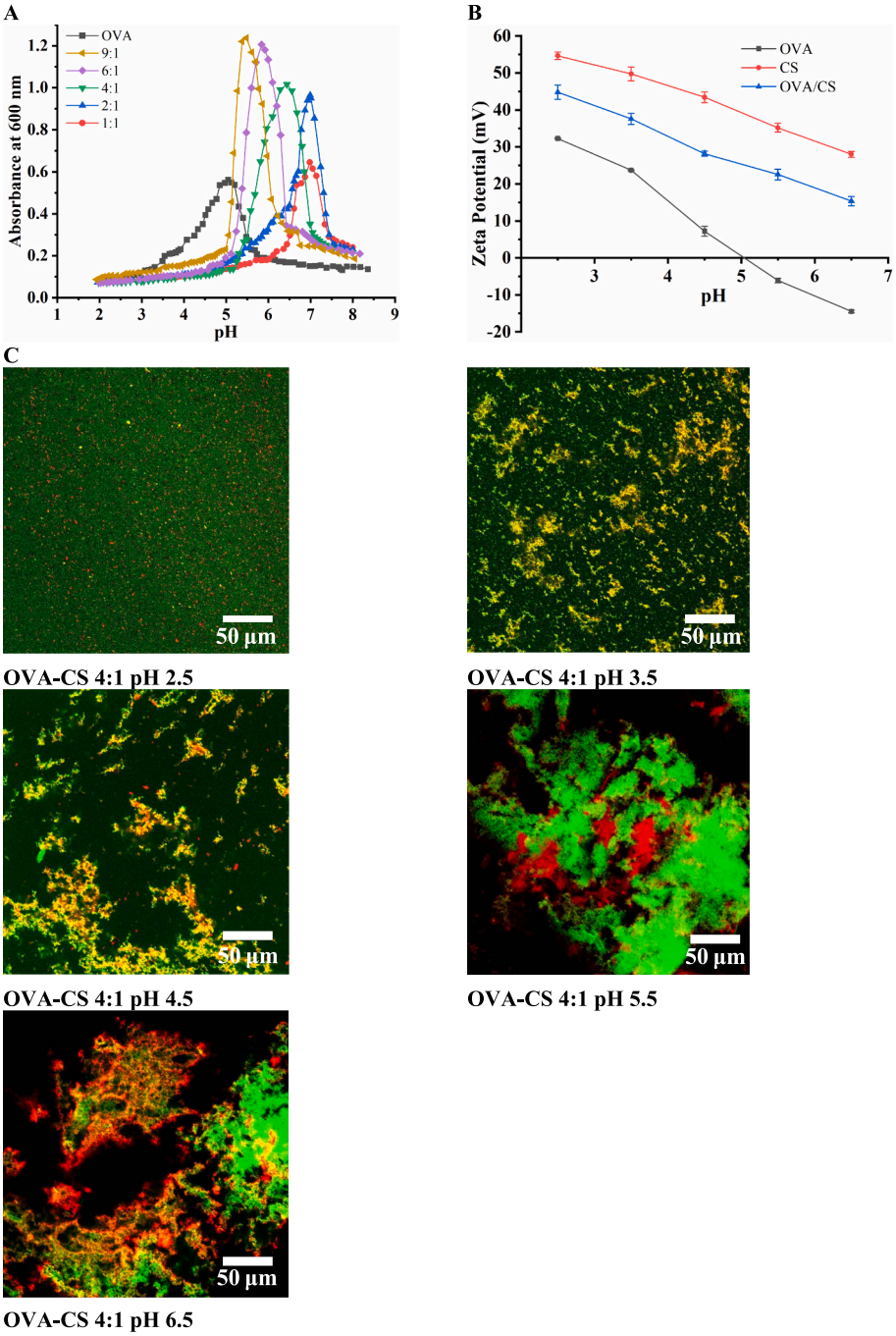

Fig. 1. The effect of OVA-CS ratio on the turbidity of OVA-CS complexes (A); The effect of pH value on the zeta-potential of OVA-CS complexes (4:1) (B); Changes of microstructure for OVA-CS complexes with different pH values (C).

pH values, reaching a maximum at the isoelectric points. This indicated the formation of insoluble complexes (coacervate) between OVA and CS at these points, with no further turbidity increase beyond them (Fig. 1A). Isoelectric points for OVA and CS (9:1, 6:1, and 4:1) were approximately pH 5.48, pH 5.84, and pH 6.44, respectively. The neutralization of surface charges led to OVA and CS aggregation, as evident from increased particle size and turbidity. Decreasing OVA concentration correlated with a gradual reduction in maximum turbidity, suggesting that the self-association and aggregation of OVA alone contributed to high turbidity values.

For OVA and CS at a mass ratio of 2:1 and 1:1, the isoelectric point was unaffected by the OVA ratio. Turbidity peaked at pH 7.0, followed by a decline (Fig. 1A). This aggregation was primarily due to the bridging effects of the OVA molecule between CS molecules, given the relatively low concentration of OVA molecules interacting with CS. At lower pH values, stability was maintained due to strong electrostatic repulsion among OVA and CS molecules. However, an increase in pH value led to the formation of OVA and CS aggregates, driven by decreasing electrostatic repulsions. At pH 7.0, electrostatic repulsions were nearly zero, resulting in maximum aggregation. Further pH increases caused the dissociation of OVA and CS aggregates, leading to CS molecule precipitation. Two distinct phases formed: one with soluble OVA molecules and another with insoluble CS.

3.1.2. Diameter and surface charge

In Fig. 1B, the isoelectric point of OVA is depicted at approximately pH 5.05, aligning with previous research findings. OVA carries a negative charge above pH 5.05, and as the pH value increases, the zeta-potential value of CS decreases, indicating the neutralization of amino groups in CS. Conversely, OVA becomes positively charged under acidic conditions. Positive charges are observed in OVA-CS complexes (OVA: CS mass ratios of 4:1) within the pH range of 2.5–6.5. Despite the weak interactions between the positively charged OVA and CS polymers, minor zeta-potential changes are noted for OVA-CS complexes in the pH range of 2.5–6.5.

Table 1 illustrates the *Z*-average particle sizes of OVA-CS complexes within the pH range of 2.5–6.5. At pH 2.5, the Z-average diameter of the OVA-CS complex (4:1) is 843.5 ± 18.6 nm, contrasting with OVA's diameter of approximately 283.1 ± 12.9 nm. Electrostatic repulsion maintains the particle size when the pH shifts from 3.5 to 4.5. However, a notable increase in particle size occurs as the pH value escalates from 5.5 to 6.5. At pH 6.5, the aggregation of the OVA-CS complex and the formation of CS aggregates cause a rapid increase in particle size due to the reduced water-solubility of CS and the diminished electrostatic interaction between OVA and CS.

3.1.3. Microstructure change

The morphology and microstructure of the OVA-CS complex (4:1) were investigated across the pH range of 2.5–6.5, as depicted in Fig. 1C. At pH 2.5, the OVA-CS complex (4:1) exhibited a spherical shape, evenly dispersed in the solution, with diameters ranging from 800 to 1000 nm, consistent with DLS results. Notably, the CLSM image revealed maximal aggregation and irregular shapes of OVA-CS complexes at relatively higher pH values (5.5 and 6.5), in line with findings by Paliya et al. (Paliya et al., 2023).

Table 1
Particle size of OVA and OVA-CS at different pH.

pH	2.5	3.5	4.5	5.5	6.5
OVA	283.1 ± 12.9^{e}	347.7 ± 5.0^{d}	390.5 ± 8.7^{c}	13,356.7 ± 110.2^{a}	760.8 ± 4.1^{b}
OVA-CS	843.5 ± 18.6^{e}	905.3 ± 15.4^{d}	925.7 ± 6.9^{c}	1381.0 ± 53.8^{b}	16,610.0 ± 325.1^{a}

All data in the table are in nm.
Different letters represent significant differences between the same line.

3.1.4. Emulsifying properties

The investigation of EAIs and ESIs of OVA-CS complexes (9:1, 6:1, 4:1, 2:1, and 1:1) in the pH range of 2.5–6.5 is presented in Fig. 2A-B. OVA (1%, *w/v*) served as the control. The OVA-CS complex (4:1) at pH 2.5 displayed the highest EAI value of 5.66 m^2/g, attributed to its optimal solubility and uniformity. An increase in pH from 2.5 to 6.5 resulted in a decline in EAI due to reduced solubility and uniformity. At pH 5.5 (near the isoelectric point), OVA exhibited the lowest EAI (0.92 m^2/g), which increased with a further rise in pH from 5.5 to 6.5.

Non-adsorbing OVA-CS complexes in the emulsion's continuous phase induced enhanced attractive interactions between droplets, leading to droplet flocculation and a rapid growth in serum layer thickness. Consequently, this caused a decrease in EAIs of OVA-CS complexes. The EAI of OVA at pH 2.5 significantly increased after CS complexation, likely linked to improved solubility. EAI values for OVA-CS complexes were 1.16 m^2/g, 2.57 m^2/g, 5.66 m^2/g, 4.44 m^2/g, and 3.00 m^2/g for mass ratios of 9:1, 6:1, 4:1, 2:1, and 1:1, respectively, influenced by OVA-CS ratio, interfacial film thickness, charge, and rigidity. The EAI, in general, correlates positively with protein water solubility (Li et al., 2022).

In the pH range of 2.5–4.5, the OVA-CS complex (4:1) demonstrated the highest EAI among all OVA-CS complexes, surpassing that of OVA alone. Notably, no significant EAI change occurred for all OVA-CS complexes with an increase in pH from 4.5 to 6.5. In the 9:1 to 4:1 ratio range, a positive correlation between CS concentration and EAI was observed for all OVA-CS complexes at pH 2.5, attributed to increased electrostatic repulsion and interface layer thickness. However, at the 2:1 and 1:1 ratios, EAI sharply decreased at pH 2.5 due to the absence of OVA.

Fig. 2B presents ESI values for OVA-CS complexes, revealing dependence on mass ratio and pH. At pH 6.5, OVA exhibited a higher ESI than all OVA and CS mixtures, indicating self-association of OVA molecules. At pH 2.5, 3.5, and 4.5, OVA-CS complexes showed higher ESI than OVA alone, suggesting synergistic effects of OVA and CS, leading to enhanced emulsion stability. The presence of CS increased the viscosity of the O/W emulsion system and emulsion stability. At pH 2.5, the ESIs of OVA-CS complexes (9:1, 6:1, and 4:1) were directly proportional to the amount of CS, while the ESIs of OVA-CS complexes (2:1 and 1:1) were inversely proportional to the amount of CS, indicating reduced emulsion stability at mass ratios of 2:1 and 1:1 due to insufficient OVA. This destabilization is attributed to bridging flocculation, consistent with previous findings on the role of ι-carrageenan in inducing flocculation in emulsions stabilized with BSA. The interaction between OVA and CS significantly enhances emulsifying activity and stability, aligning with previous research results (He et al., 2021).

3.1.5. Interfacial adsorption properties

The adsorption of the protein-polysaccharide complex onto oil droplets is primarily influenced by decreased interfacial tension, a key physical parameter. Fig. 2C-D presents the exploration of interfacial tensions for OVA and OVA-CS complexes at different pH values. All samples exhibited an initial steep slope followed by a nearly horizontal second slope over time. At pH 2.5, the initial interfacial tension of OVA was 15.98 mN/m, which reduced to 12.49 mN/m upon the addition of CS. The highest interfacial tension for OVA (19.28 mN/m) was observed at pH 5.5, corresponding to the lowest emulsifying activity. This was attributed to pronounced OVA aggregation, limiting adsorption and film formation at the oil-water interface. Both decreasing and increasing pH values from 5.5 decreased the interfacial tension of OVA. In contrast, the interfacial tensions of OVA-CS complexes (4:1) were lower than that of OVA alone at pH 4.5, 5.5, and 6.5, with CS contributing to a more substantial decrease.

The addition of CS led to a greater reduction in interfacial tensions, enhancing the thermodynamic stability of emulsions. Complexation of OVA-CS resulted in the partial unfolding of OVA, exposing hydrophobic groups and increasing adsorption to the oil-water interface. This

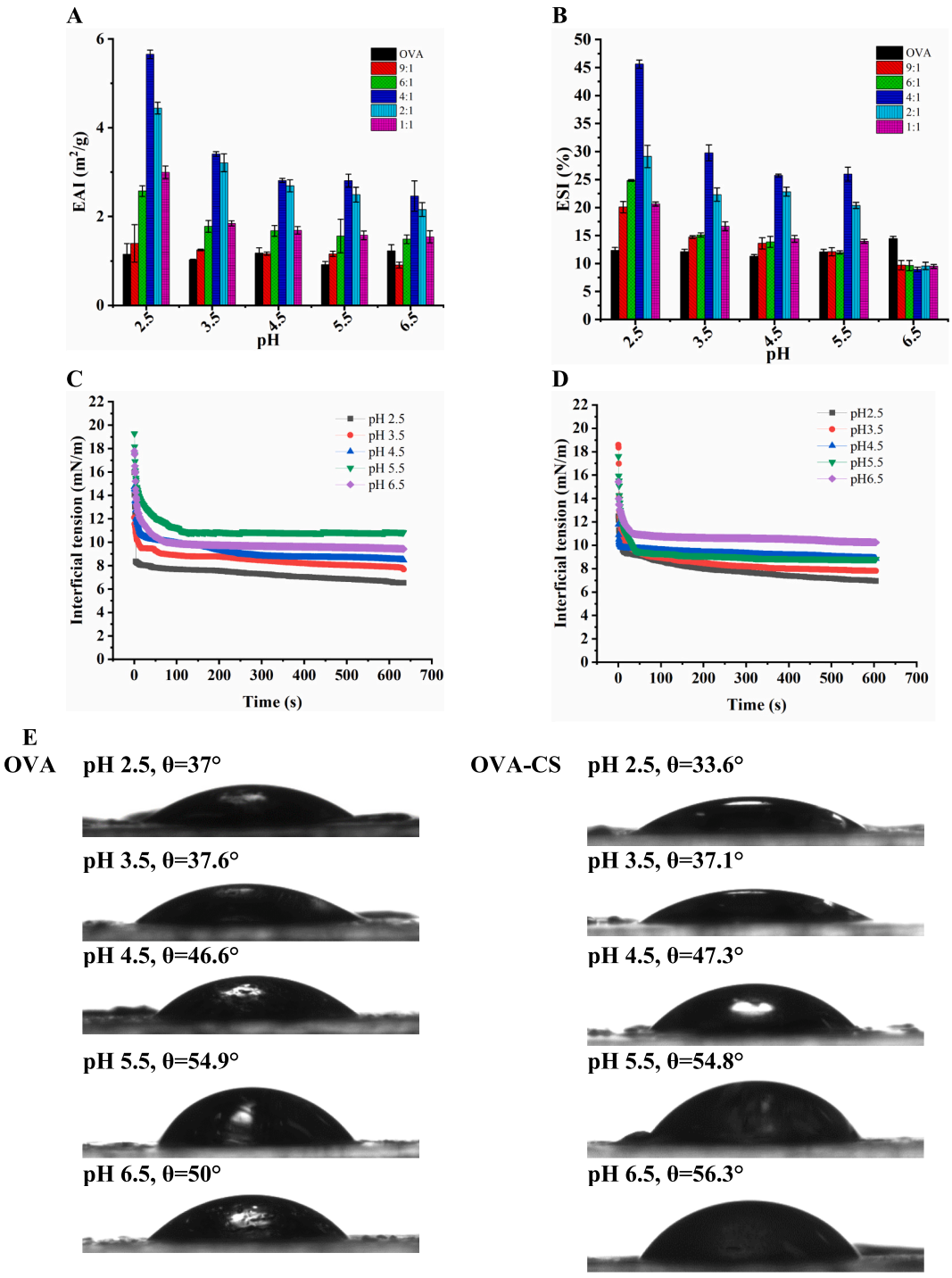

Fig. 2. OVA-CS complexes emulsifying activity (A); OVA-CS complexes emulsifying stability (B); Changes of interfacial tension with time for OVA (C) and OVA-CS complexes (D) with different pH values; Changes of contact angle for OVA and OVA-CS complexes with different pH values (E).

increased hydrophobicity facilitates OVA adsorption, with a strong positive correlation between surface hydrophobicity and protein emulsifying activity. Higher CS concentrations may expose more interior hydrophobic amino acid residues of OVA. Despite this, a strong negative exponential relationship between interfacial tension and emulsifying activity was observed, emphasizing the strengthening of emulsifying activity with decreasing interfacial tension, in line with previous studies. CS enhances the emulsifying activity of OVA by increasing hydrophobicity, water-solubility, and protein adsorption at the oil-water interface of OVA-CS complexes. This finding aligns with the measurement of contact angles in Fig. 2E, where the θ of OVA-CS complexes was 56.3°, indicating stronger hydrophobicity. During the acidification process, θ gradually decreased from 56.3° to 33.6°, suggesting that an adequate pH value could improve the hydrophobicity of OVA-CS complexes. While OVA-CS complexes exhibited lower hydrophobicity than OVA, at pH 2.5, they demonstrated the most suitable wettability, implying their potential as ideal stabilizers for preparing HIPEs.

3.2. Structural characteristics of lycopene-loaded HIPEs stabilized by OVA-CS complexes

3.2.1. Macroscopic appearance

The encapsulation of lycopene within OVA-CS-stabilized HIPEs involved mixing the lycopene oil phase with the OVA-CS aqueous dispersion. OVA-stabilized HIPEs containing lycopene were utilized as a control. These HIPEs were constructed with an internal phase volume fraction of 75%. Fig. 3A and B illustrate that post-encapsulation, the color of the HIPEs turned orange, indicating the successful encapsulation of lycopene within the structures. Notably, 3% OVA-CS-stabilized HIPEs exhibited an outstanding encapsulating capacity, reaching up to 0.4% lycopene, surpassing the 0.3% achieved by 3% OVA-stabilized HIPEs (Fig. 3A).

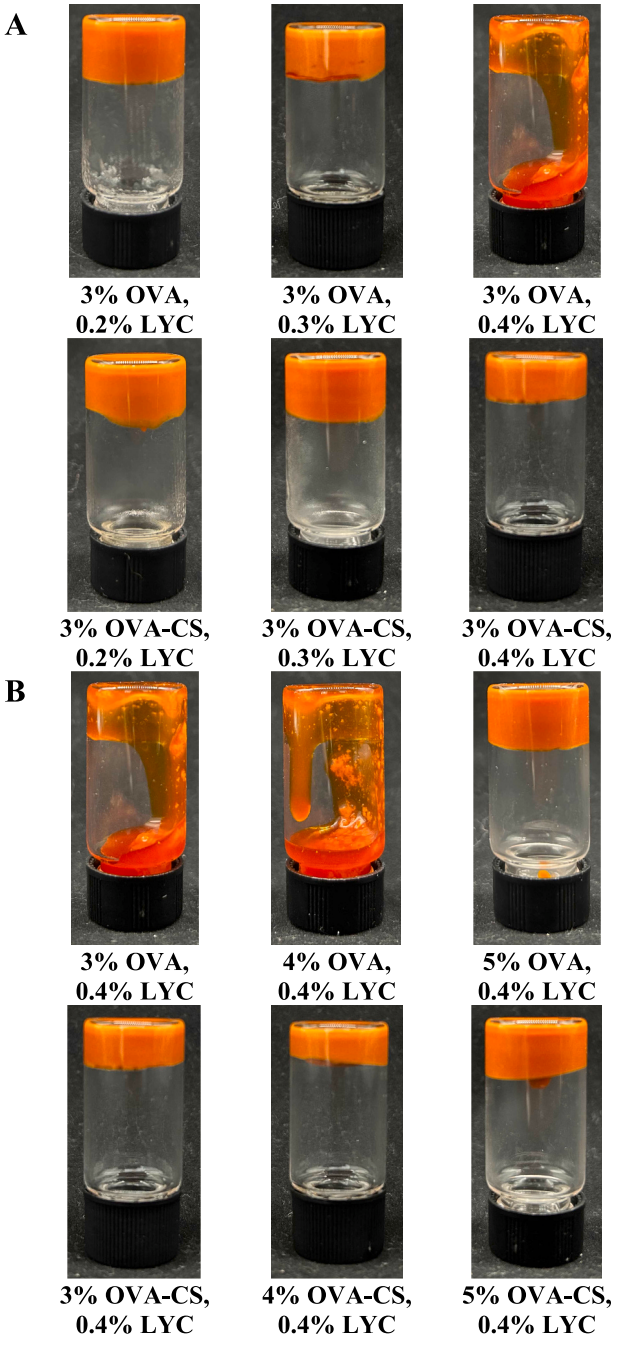

Fig. 3. HIPEs encapsulated different concentrations of lycopene with 3% OVA and 3% OVA-CS complexes (φ = 0.75) (A); HIPEs encapsulated 0.4 wt% lycopene with different mass concentrations of OVA and OVA-CS complexes (φ = 0.75) (B).

Comparatively, Zhao et al. achieved a maximum encapsulation of 0.2% lycopene using lactoferrin-stabilized emulsion at an internal phase volume fraction of 10% (Zhao et al., 2020). Fig. 3B further demonstrates that OVA-CS stabilized HIPEs displayed an ability to encapsulate 0.4% lycopene with mass concentrations of the OVA-CS complex ranging from 3% to 5%. In contrast, OVA-stabilized HIPEs achieved the encapsulation of 0.4% lycopene with a mass concentration of OVA up to 5%. This indicates that the OVA-CS complex enhances the encapsulation ability of OVA alone for lycopene, allowing for an increase in the oil phase ratio of HIPEs up to 75% and the concentration of lycopene in the oil phase up to 0.4%.

3.2.2. Particle size

Table 2 indicates that the smallest droplet size was observed in the 5% OVA-CS, 0.4% LYC group, while the largest droplet size was found in the 3% OVA-CS, 0.2% LYC group. In Fig. 4, a comparison with the control group (3% OVA, 0.2% LYC group, 3% OVA, 0.3% LYC group, and 5% OVA, 0.4% LYC group) reveals that the oil droplets in the OVA-CS 3 groups were smaller, uniformly distributed, and tightly packed, consistent with the particle size measurement results. This outcome indicates that the structural strength of the gel network formed by the OVA-CS complex is higher than that of OVA alone, and this characteristic is concentration-dependent.

3.2.3. Encapsulation efficiency and loading capacity

The HPLC-DAD chromatogram at 471 nm of an isomerized (all-*E*)-lycopene extracted from lycopene oil was shown in Fig. S1. The identification of lycopene isomers was confirmed by comparison with reported data in the literature, including UV–Vis spectral data, retention times, *Z*-peak (the peak at approximately 360 nm, characteristic peak of lycopene isomers, shown in Fig. S2), Q value (DB/DII, DB: the maximum height of the *Z*-peak, DII: the maximum height of the main absorption peak, shown in Fig. S2). According to previous work in reference (Phan-Thi & Waché, 2014; Sun et al., 2016; Yang et al., 2021), the peak identification results can be seen in Table S1. The spectra of the main isomers of lycopene were shown in Fig. S3. The main difference between *Z*-lycopene and (all-*E*)-lycopene is the appearance of a *Z*-peak in the near-ultraviolet region, and the intensity of the *Z*-peak increases as the *Z*-double bond is closer to the center of the molecule. Additionally, *Z*-lycopene have the relative blueshifts of the maximum absorption wavelength of approximately 5–10 nm in comparison to (all-*E*)-lycopene.

Lycopene was encapsulated in HIPEs stabilized by varying mass concentrations of OVA-CS complexes, with lycopene-loaded HIPEs stabilized by corresponding mass concentrations of OVA serving as a control. Fig. 5A reveals that the EE for all samples ranged from 97.50% to 98.19%, with no significant differences. Given the excellent EE of HIPEs,

Table 2
Particle size of OVA and OVA-CS stabilized HIPEs with lycopene.

Sample	D4,3 (μm)	D3,2 (μm)	D10 (μm)	D50 (μm)	D90 (μm)
3%OVA, 0.2%LYC	62.90 ± 0.53^{a}	30.41 ± 0.35^{a}	18.42 ± 0.71^{a}	35.98 ± 0.21^{a}	246.40 ± 1.26^{a}
3%OVA, 0.3%LYC	42.14 ± 0.23^{d}	22.49 ± 0.24^{c}	13.36 ± 0.51^{b}	26.45 ± 1.24^{c}	238.00 ± 5.24^{b}
5%OVA, 0.4%LYC	37.80 ± 0.22^{e}	18.65 ± 0.11^{d}	10.21 ± 0.76^{c}	24.27 ± 3.99^{c}	147.30 ± 6.64^{c}
3%OVA-CS, 0.2%LYC	56.81 ± 0.42^{b}	25.62 ± 0.34^{b}	13.38 ± 0.93^{b}	32.42 ± 2.73^{b}	71.83 ± 4.71^{d}
3%OVA-CS, 0.3%LYC	53.42 ± 0.43^{c}	18.54 ± 0.13^{d}	9.87 ± 0.04^{d}	20.71 ± 0.23^{e}	63.84 ± 4.50^{e}
5%OVA-CS, 0.4%LYC	34.84 ± 0.16^{f}	17.32 ± 0.09^{e}	8.90 ± 0.04^{e}	21.12 ± 0.35^{d}	50.16 ± 6.22^{f}

Different letters represent significant differences between the same column.

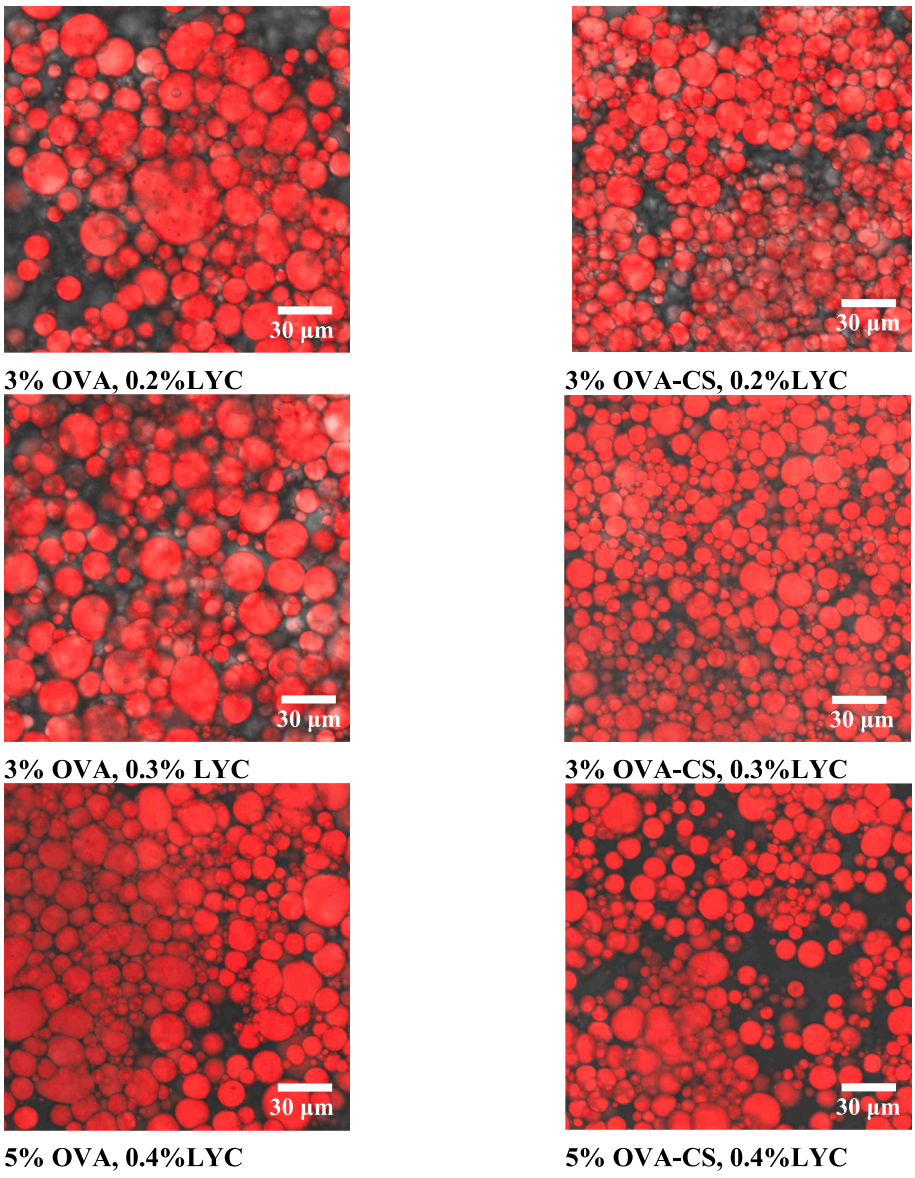

Fig. 4. The microstructure of lycopene-loaded HIPEs.

the LA of lycopene in HIPEs depended on the concentration of lycopene in corn oil. The LA values for lycopene in the 3% OVA-CS, 0.2% LYC group, the 3% OVA-CS, 0.3% LYC group, and the 5% OVA-CS, 0.4% LYC group were 1.1850 mg/g, 1.4532 mg/g, and 1.7661 mg/g, respectively (Fig. 5A). Higher concentrations of lycopene in corn oil resulted in increased LA of lycopene in HIPEs.

3.3. The storage stability of lycopene-loaded HIPEs stabilized by OVA-CS complexes

The retention rates of lycopene in HIPEs encapsulated by OVA and OVA-CS complexes during 30 days of storage at 25 °C, 45 °C, 80 °C, and 25 °C with light are depicted in Fig. 5B-5E. Lycopene-loaded corn oil served as the control. As the storage time increased, lycopene's retention rate in all samples gradually decreased. Lycopene degraded more slowly at 25 °C than at higher temperature (45 °C and 80 °C) because the free radicals produced by oil oxidation accelerated the degradation of lycopene at higher temperatures. From the results obtained, it was clear that the OVA-CS encapsulated lycopene showed the highest lycopene degradation under all tested conditions. The retention rate of lycopene in OVA-CS HIPEs decreased significantly as the storage temperature rose, while it also decreased with light. Although storage at high temperatures (45 °C and 80 °C), the retention rate of lycopene was still up to 65.37% and 41.82% respectively after 30 days, which is much higher than that in oil. Thus, it demonstrates that the OVA-CS HIPEs can effectively inhibit the degradation of lycopene during storage. This result is not surprising because most of biomacromolecule-stabilized HIPEs can provide a protective effect for encapsulated cargos (Jain et al., 2020). Approximately 40% of lycopene in corn oil was lost after only 10 days of storage, and over 80% degraded after 30 days, indicating rapid degradation. The retention rate of lycopene in OVA-stabilized HIPEs remained up to ~65% after 30 days, significantly higher than lycopene in corn oil. This highlights the effective inhibition of lycopene degradation during storage by OVA-stabilized HIPEs.

Remarkably, almost 98.2% of lycopene was retained in the 5% OVA-CS-stabilized HIPEs after 30 days of storage, surpassing OVA-stabilized HIPEs and lycopene-dispersed oil samples. Furthermore, compared to lycopene-loaded electrospun nanofibers stored at 4 °C, the lycopene retention rate in 5% OVA-CS-stabilized HIPEs stored at 25 °C was comparable (Chen, Xiang, et al., 2023). The retention rate was 65.26% for 5% OVA-stabilized HIPEs after 30 days, while it slowly decreased to 97.22% with 5% OVA-CS complexes ($P < 0.05$). The larger oil droplet

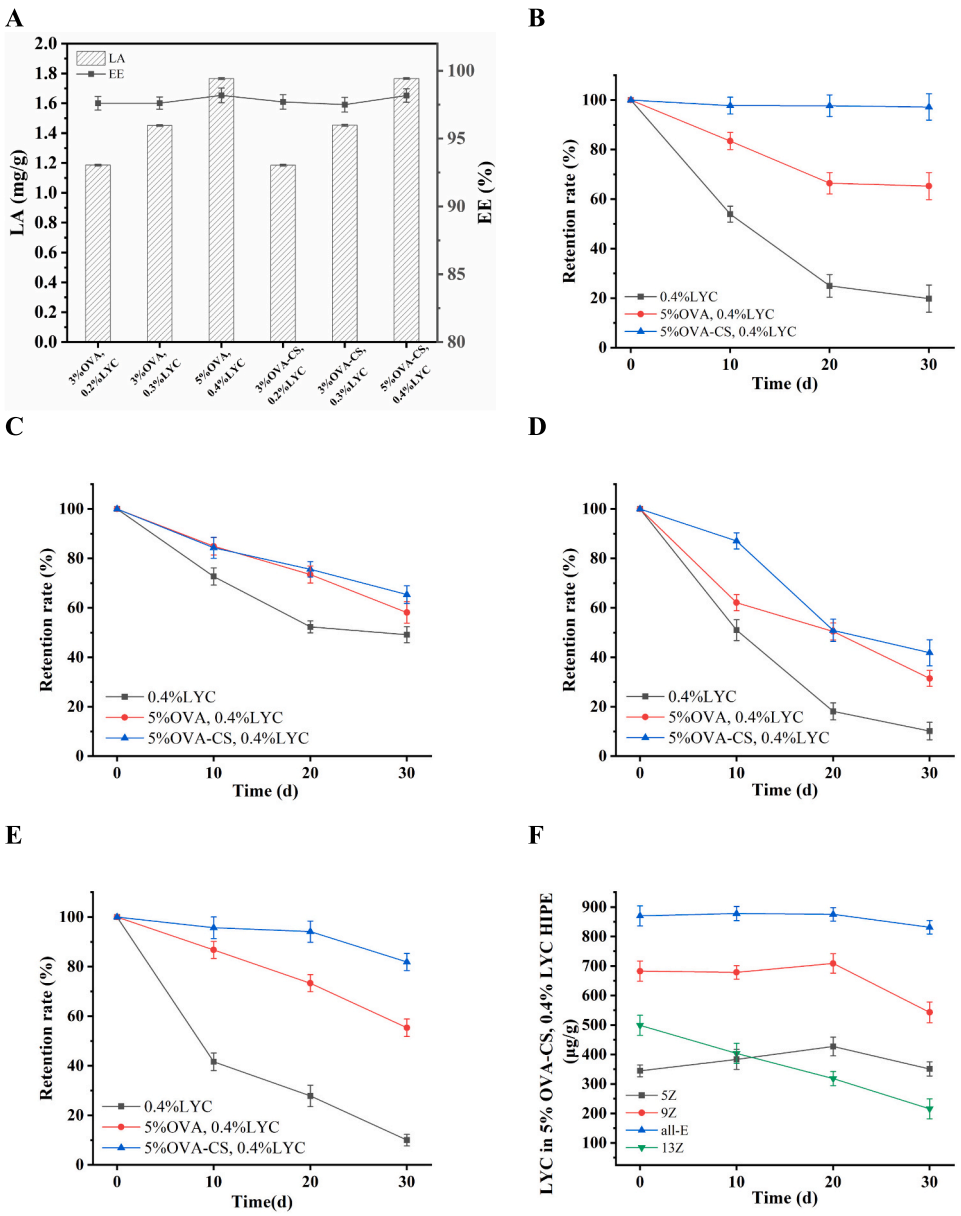

Fig. 5. Encapsulation efficiency (EE) and loading capacity (LA) of lycopene in HIPEs (A); Retention rate of lycopene at 25 °C (B), 45 °C (C), 80 °C (D), and 25 °C with light (E) during 30 d storage; Content of lycopene configuration in the 5%OVA-CS, 0.4%LYC group varied at 25 °C during 30 d storage (F).

diameter (50.16 μm) and bigger interfacial area in our study may contribute to better protection compared to HIPE (20.0 μm) by H. Chen et al. (Chen, Sun, et al., 2023). The enhanced retention in 5% OVA-CS-stabilized HIPEs is attributed to the vital role of the interfacial layer formed with OVA-CS complexes, acting as a physical barrier against the interaction between lycopene and pro-oxidants. Additionally, the increased oil fraction contributes to improved emulsion viscosity, enhancing oxygen isolation. The excellent stability of lycopene in HIPE stabilized by OVA-CS complexes can be directly reflected in Fig. 5E. Fig. 5F reveals the identification of (13*Z*)-, (9*Z*)-, (5*Z*)-, and (all-*E*)-lycopene in the 5% OVA-CS, 0.4% LYC group. Compared with (9*Z*)- and (13*Z*)-lycopene, (all-*E*)- and (5*Z*)-lycopene are more stable under light irradiation, because lycopene molecules with *Z*-double bonds in the outer part of the conjugated chain (such as (5*Z*)-lycopene) are more stable than lycopene molecules with *Z*-double bonds in the central part of the conjugated chain (such as (9*Z*)- and (13*Z*)-lycopene). The concentrations of (13*Z*)-, (9*Z*)-, and (5*Z*)-lycopene declined slightly, indicating that the 5% OVA-CS-stabilized HIPEs exert a protective effect on the *Z*-lycopene (Honda, 2023; Yang et al., 2021).

4. Conclusion

In conclusion, the successful fabrication of spherical and homogeneously dispersed OVA-CS complexes at a pH of 2.5 with mass ratios of 4:1 demonstrates their excellent emulsifying properties, making them ideal stabilizers for the preparation of HIPEs. The EE of lycopene within the OVA-CS stabilized HIPEs was found to be 98.19%, with a lycopene LA of 1.7661 mg/g. Moreover, the encapsulation endows the lycopene with superior storage stability (25 °C, 45 °C and 80 °C) and UV stability (25 °C with light). After storage for 30 days with light, the retention of lycopene in OVA-CS HIPEs reached 81.86%, and its content in the *Z*-lycopene only showed a slight decrease. This remarkable preservation can be attributed to the formation of a thick interface layer over the oil droplets due to the high mass concentration of OVA-CS complexes. This layer led to a decrease in the average size of the oil droplets within the HIPEs, resulting in a tighter packing of the droplets. These effects

effectively minimized the impact of the external environment on the activity of lycopene. Based on these findings, the OVA-CS stabilized HIPE encapsulation system exhibits tremendous potential as an alternative and efficient approach for delivering lycopene in the food and pharmaceutical industries. Additionally, these results provide valuable insights into the potential utilization of biopolymer-based HIPEs for the encapsulation, protection, and encapsulation of hydrophobic nutraceuticals. This information is highly useful for the development of nutraceuticals and functional foods. In future studies, investigating the in-vivo gastrointestinal fate of this encapsulation system will further enhance our understanding of its mechanisms and contribute to its practical application.

Funding

This work was supported by the grants from Thirteen Five National Key Research and Development Program of China (2018YFD0400902), Changji science and technology project (2019G02).

CRediT authorship contribution statement

Dan Wang: Writing – review & editing, Writing – original draft, Methodology, Investigation, Funding acquisition, Data curation. **Junmiao Zhang:** Validation, Supervision, Methodology, Formal analysis. **Lei Zhong:** Validation, Supervision, Software, Resources. **Cheng Yang:** Supervision, Software, Resources, Funding acquisition. **Xuejian Zhang:** Supervision, Software, Resources, Funding acquisition. **Qiuhui Hu:** Writing – review & editing, Supervision, Resources, Methodology, Funding acquisition, Conceptualization. **Lianfu Zhang:** Writing – review & editing, Supervision, Resources, Methodology, Funding acquisition, Conceptualization.

Declaration of generative AI and AI-assisted technologies in the writing process

During the preparation of this work, the authors used ChatGPT in order to polish language. After using this tool, the authors reviewed and edited the content as needed and takes full responsibility for the content of the publication.

Declaration of competing interest

The authors declare that they have no known competing financial interests or personal relationships that could have appeared to influence the work reported in this paper.

Data availability

The data that has been used is confidential.

Appendix A. Supplementary data

Supplementary data to this article can be found online at https://doi.org/10.1016/j.fochx.2024.101689.

References

Banasaz, S., Morozova, K., Ferrentino, G., & Scampicchio, M. (2020). Encapsulation of lipid-soluble bioactives by nanoemulsions. *Molecules, 25*(17). https://doi.org/10.3390/molecules25173966

Chen, H., Sun, Y., Feng, X., Ma, L., Dai, H., Wang, H., Zhu, H., Yu, Y., & Zhang, Y. (2023). Thermal-induced-stable high internal phase emulsion for lycopene encapsulation and delivery: Pre-heat treatment mediated facilitation on the isomerization, stabilization, and release of lycopene. *Lwt, 187*. https://doi.org/10.1016/j.lwt.2023.115319

Chen, L., Xiang, M., Wu, F., Jiang, Y., Wu, Q., Zhang, W., Guo, W., Cai, B., Liang, L., Li, S., Chen, Y., & Du, X. (2023). Encapsulation of lycopene into electrospun nanofibers from whey protein isolate-Tricholoma lobayense polysaccharide complex stabilized emulsions: Structural characterization, storage stability, in vitro release, and cellular evaluation. *International Journal of Biological Macromolecules, 238*. https://doi.org/10.1016/j.ijbiomac.2023.123993

Chen, X., Liang, R., Zhong, F., Ma, J., John, N.-A., Goff, H. D., & Yokoyama, W. H. (2021). Effect of high concentrated sucrose on the stability of OSA-starch-based beta-carotene microcapsules. *Food Hydrocolloids, 113*. https://doi.org/10.1016/j.foodhyd.2019.105472

Falsafi, S. R., Rostamabadi, H., Babazadeh, A., Tarhan, Ö., Rashidinejad, A., Boostani, S., … Jafari, S. M. (2022). Lycopene nanodelivery systems; recent advances. *Trends in Food Science & Technology, 119*, 378–399. https://doi.org/10.1016/j.tifs.2021.12.016

Gao, H., Ma, L., Cheng, C., Liu, J., Liang, R., Zou, L., … McClements, D. J. (2021). Review of recent advances in the preparation, properties, and applications of high internal phase emulsions. *Trends in Food Science & Technology, 112*, 36–49. https://doi.org/10.1016/j.tifs.2021.03.041

Gao, J., Qiu, Y., Chen, F., Zhang, L., Wei, W., An, X., & Zhu, Q. (2023). Pomelo peel derived nanocellulose as Pickering stabilizers: Fabrication of Pickering emulsions and their potential as sustained-release delivery systems for lycopene. *Food Chemistry, 415*. https://doi.org/10.1016/j.foodchem.2023.135742

Hasanvand, E., & Razavi, S. M. A. (2023). Fabrication and characterisation of milk proteins-chitosan complex coacervates. *International Dairy Journal, 145*. https://doi.org/10.1016/j.idairyj.2023.105716

He, W., Xiao, N., Zhao, Y., Yao, Y., Xu, M., Du, H., Wu, N., & Tu, Y. (2021). Effect of polysaccharides on the functional properties of egg white protein: A review. *Journal of Food Science, 86*(3), 656–666. https://doi.org/10.1111/1750-3841.15651

Honda, M. (2023). Z-isomers of lycopene and β-carotene exhibit greater skin-quality improving action than their all-E-isomers. *Food Chemistry, 421*. https://doi.org/10.1016/j.foodchem.2023.135954

Jain, S., Winuprasith, T., & Suphantharika, M. (2020). Encapsulation of lycopene in emulsions and hydrogel beads using dual modified rice starch: Characterization, stability analysis and release behaviour during in-vitro digestion. *Food Hydrocolloids, 104*. https://doi.org/10.1016/j.foodhyd.2020.105730

Li, Y., Xu, Y., & Xu, X. (2022). Continuous cyclic wet heating glycation to prepare myofibrillar protein-glucose conjugates: A study on the structures, solubility and emulsifying properties. *Food Chemistry, 388*. https://doi.org/10.1016/j.foodchem.2022.133035

Murakami, K., Kageyama, H., Hibino, T., Zhang, Y., Goto, M., & Honda, M. (2022). Preparation of highly stable Z-isomer-rich lycopene nanodispersions via a continuous-flow system with selected emulsifiers. *European Journal of Lipid Science and Technology, 124*(8). https://doi.org/10.1002/ejlt.202200034

Mwangi, W. W., Lim, H. P., Low, L. E., Tey, B. T., & Chan, E. S. (2020). Food-grade Pickering emulsions for encapsulation and delivery of bioactives. *Trends in Food Science & Technology, 100*, 320–332. https://doi.org/10.1016/j.tifs.2020.04.020

Nazemiyeh, E., Eskandani, M., Sheikhloie, H., & Nazemiyeh, H. (2016). Formulation and physicochemical characterization of lycopene-loaded solid lipid nanoparticles. *Advanced Pharmaceutical Bulletin, 6*(2), 235–241. https://doi.org/10.15171/apb.2016.032

Paliya, B. S., Sharma, V. K., Sharma, M., Diwan, D., Nguyen, Q. D., Aminabhavi, T. M., … Gupta, V. K. (2023). Protein-polysaccharide nanoconjugates: Potential tools for delivery of plant-derived nutraceuticals. *Food Chemistry, 428*. https://doi.org/10.1016/j.foodchem.2023.136709

Phan-Thi, H., & Waché, Y. (2014). Isomerization and increase in the antioxidant properties of lycopene from *Momordica cochinchinensis* (gac) by moderate heat treatment with UV–vis spectra as a marker. *Food Chemistry, 156*, 58–63. https://doi.org/10.1016/j.foodchem.2014.01.040

Rehman, A., Liang, Q., Karim, A., Assadpour, E., Jafari, S. M., Rasheed, H. A., … Ren, X. (2024). Pickering high internal phase emulsions stabilized by biopolymeric particles: From production to high-performance applications. *Food Hydrocolloids, 150*. https://doi.org/10.1016/j.foodhyd.2024.109751

Rostamabadi, H., Falsafi, S. R., & Jafari, S. M. (2019). Nanoencapsulation of carotenoids within lipid-based nanocarriers. *Journal of Controlled Release, 298*, 38–67. https://doi.org/10.1016/j.jconrel.2019.02.005

Saini, R. K., Rengasamy, K. R. R., Mahomoodally, F. M., & Keum, Y.-S. (2020). Protective effects of lycopene in cancer, cardiovascular, and neurodegenerative diseases: An update on epidemiological and mechanistic perspectives. *Pharmacological Research, 155*. https://doi.org/10.1016/j.phrs.2020.104730

Saini, R. K. A., Bekhit, A. E. D., Roohinejad, S., Rengasamy, K. R. R., & Keum, Y.-S. (2019). Chemical stability of lycopene in processed products: A review of the effects of processing methods and modern preservation strategies. *Journal of Agricultural and Food Chemistry, 68*(3), 712–726. https://doi.org/10.1021/acs.jafc.9b06669

Sampaio, G. L. A., Pacheco, S., Ribeiro, A. P. O., Galdeano, M. C., Gomes, F. S., & Tonon, R. V. (2019). Encapsulation of a lycopene-rich watermelon concentrate in alginate and pectin beads: Characterization and stability. *Lwt, 116*. https://doi.org/10.1016/j.lwt.2019.108589

Sharkawy, A., Barreiro, M. F., & Rodrigues, A. E. (2020). Chitosan-based Pickering emulsions and their applications: A review. *Carbohydrate Polymers, 250*. https://doi.org/10.1016/j.carbpol.2020.116885

Sharma, S., Sathasivam, T., Rawat, P., & Pushpamalar, J. (2021). Lycopene-loaded nanostructured lipid carrier from carboxymethyl oil palm empty fruit bunch cellulose for topical administration. *Carbohydrate Polymer Technologies and Applications, 2*. https://doi.org/10.1016/j.carpta.2021.100049

Sun, Q., Yang, C., Li, J., Raza, H., & Zhang, L. (2016). Lycopene: Heterogeneous catalytic E/Z isomerization and in vitro bioaccessibility assessment using a diffusion model. *Journal of Food Science, 81*(10). https://doi.org/10.1111/1750-3841.13419

Sun, Y., Zhong, M., Sun, Y., Li, Y., Qi, B., & Jiang, L. (2022). Stability and digestibility of encapsulated lycopene in different emulsion systems stabilized by acid-modified

soybean lipophilic protein. *Journal of the Science of Food and Agriculture, 102*(13), 6146–6155. https://doi.org/10.1002/jsfa.11968

Thareja, P., Saraswat, Y. C., & Oberoi, C. (2020). Ovalbumin-stabilized concentrated emulsion gels. *Bulletin of Materials Science, 43*(1). https://doi.org/10.1007/s12034-020-02163-x

Wang, L., Li, Y. J., Xiang, D., Zhang, W. M., & Bai, X. P. (2020). Stability of lutein in O/W emulsion prepared using xanthan and propylene glycol alginate. *International Journal of Biological Macromolecules, 152*, 371–379. https://doi.org/10.1016/j.ijbiomac.2020.02.162

Wang, Q., Yang, C., Liu, Y., Zhang, J., & Zhang, L. (2022). Efficient E/Z conversion of (all-E)-lycopene to Z-isomers with a high proportion of (5Z)-lycopene by metal salts. *Lwt, 160*. https://doi.org/10.1016/j.lwt.2022.113268

Wei, Y., Zhou, D., Mackie, A., Yang, S., Dai, L., Zhang, L., … Gao, Y. (2021). Stability, interfacial structure, and gastrointestinal digestion of β-carotene-loaded Pickering emulsions co-stabilized by particles, a biopolymer, and a surfactant. *Journal of Agricultural and Food Chemistry, 69*(5), 1619–1636. https://doi.org/10.1021/acs.jafc.0c06409

Xia, S., Wang, Q., Rao, Z., Lei, X., Zhao, J., Lei, L., & Ming, J. (2024). High internal phase Pickering emulsions stabilized by zein/whey protein nanofibril complexes: Preparation and lycopene loading. *Food Chemistry, 452*, Article 139564. https://doi.org/10.1016/j.foodchem.2024.139564

Xiong, W., Ren, C., Tian, M., Yang, X., Li, J., & Li, B. (2017). Complex coacervation of ovalbumin-carboxymethylcellulose assessed by isothermal titration calorimeter and rheology: Effect of ionic strength and charge density of polysaccharide. *Food Hydrocolloids, 73*, 41–50. https://doi.org/10.1016/j.foodhyd.2017.06.031

Xu, Y. T., Yang, T., Liu, L. L., & Tang, C. H. (2020). One-step fabrication of multifunctional high internal phase Pickering emulsion gels solely stabilized by a softer globular protein nanoparticle: S-ovalbumin. *Journal of Colloid and Interface Science, 580*, 515–527. https://doi.org/10.1016/j.jcis.2020.07.054

Yang, C., Jiang, X., Ma, L., Xiong, W., Zhang, S., Zhang, J., & Zhang, L. (2021). Carotenoid composition and antioxidant activities of Chinese orange-colored tomato cultivars and the effects of thermal processing on the bioactive components. *Journal of Food Science, 86*(5), 1751–1765. https://doi.org/10.1111/1750-3841.15682

Yao, X., McClements, D. J., Su, Y., Li, J., Chang, C., Wang, J., … Gu, L. (2022). Fabrication, structural and emulsifying properties of egg white protein-dextran conjugates through Maillard reaction. *Food Biophysics, 17*(4), 650–661. https://doi.org/10.1007/s11483-022-09745-8

Zahari, C. N. M. C., Mohamad, N. V., Akinsanya, M. A., & Gengatharan, A. (2023). The crimson gem: Unveiling the vibrant potential of lycopene as a functional food ingredient. *Food Chemistry Advances, 3*. https://doi.org/10.1016/j.focha.2023.100510

Zhang, J., Zhao, S., Liu, Q., Chen, Q., Liu, H., & Kong, B. (2023). High internal phase emulsions stabilized by pea protein isolate modified by ultrasound and pH-shifting: Effect of chitosan self-assembled particles. *Food Hydrocolloids, 141*. https://doi.org/10.1016/j.foodhyd.2023.108715

Zhao, C., Wei, L., Yin, B., Liu, F., Li, J., Liu, X., Wang, J., & Wang, Y. (2020). Encapsulation of lycopene within oil-in-water nanoemulsions using lactoferrin: Impact of carrier oils on physicochemical stability and bioaccessibility. *International Journal of Biological Macromolecules, 153*, 912–920. https://doi.org/10.1016/j.ijbiomac.2020.03.063

Zhao, Q., Gu, Q., Hong, X., Liu, Y., & Li, J. (2021). Novel protein-based nanoparticles from perilla oilseed residues as sole Pickering stabilizers for high internal phase emulsions. *Lwt, 145*. https://doi.org/10.1016/j.lwt.2021.111340

Zou, Y., Sun, Q., Li, J., Yang, C., Yang, J., & Zhang, L. (2014). Effects of E/Z isomers of lycopene on experimental prostatic hyperplasia in mice. *Fitoterapia, 99*, 211–217. https://doi.org/10.1016/j.fitote.2014.09.013